Acta Geotechnica (2021) 16:2291–2299
https://doi.org/10.1007/s11440-021-01145-5

SHORT COMMUNICATION

Shear fracture energies of stiff clays and shales

Jinhyun Choo[1] · Ammar Sohail[1] · Fan Fei[1] · Teng-fong Wong[2]

Received: 15 October 2020 / Accepted: 10 January 2021 / Published online: 7 February 2021

Abstract
Fracture mechanics analysis of shear band propagation requires knowledge of the material's shear fracture energy and its related properties such as the characteristic slip displacement. Yet these properties of stiff clays and shales have not been investigated systematically. This work characterizes and analyzes the shear fracture energies and characteristic slip displacements of various stiff clays and shales based on their triaxial compression data from the literature. A methodology originally developed for hard rocks was adopted for this purpose. Results show that the shear fracture energies of stiff clays and shales generally increase with the effective normal stress on the slip plane, varying by orders of magnitude—approximately from 4×10^1 to 7×10^3 J/m^2—in the range of effective normal stresses from 10^2 to 10^5 kPa. An empirical equation is presented for a first-order estimate of the shear fracture energy under a given effective normal stress. The characteristic slip displacements at the laboratory scale are calculated to be smaller than 6 mm, and they appear independent of the effective normal stress. Compared with their nominal values calculated without considering the change of normal stress in triaxial tests, the shear fracture energies are approximately 70% of the nominal values, whereas the characteristic slip displacements are nearly identical to the nominal ones.

Keywords Fracture mechanics · Progressive failure · Shales · Shear band · Slip surfaces · Stiff clays

1 Introduction

Shear failures in brittle geomaterials are associated with localization of deformation into narrow zones, which are called shear bands in general, and slip surfaces in soil mechanics. Mathematically, the onset of shear band localization has been well described by bifurcation analysis [1, 2]. Nevertheless, the propagation of a shear band, which is beyond the scope of bifurcation analysis, is also important for many problems. A representative example is progressive failure in low-permeability geomaterials such as clays and shales.

Over the decades, a number of researchers have studied the application of fracture mechanics principles to understand and analyze the propagation of shear bands in geomaterials. Skempton [3], Bjerrum [4], and Bishop [5] were the first to suggest and apply fracture mechanics concepts to slip surface growth in progressive failure. Later, Palmer and Rice [6] formulated a fracture mechanics theory for the growth of a shear band, deriving conditions for propagation. Since 2004, Puzrin and coworkers have pioneered the shear band propagation approach, whereby a generalized version of Palmer and Rice's theory is applied to slope stability analyses [7–10]. Quinn et al. [11, 12] have also used the theory of Palmer and Rice to study progressive failure in sensitive clays. Meanwhile, Viesca and Rice [13] have extended the theory to slip surface growth triggered by localized increase of pore pressure, providing insight into the initiation of submarine landslides under various conditions. Very recently, Fei and Choo [14, 15] have developed a numerical method that can simulate a shear banding process from initiation to propagation, by incorporating Palmer and Rice's theory into phase-field modeling of fracture. Thanks to these advances, fracture mechanics can now be applied to a variety of geotechnical problems that involve shear banding.

Fracture mechanics analysis of shear bands requires knowledge of the material's shear fracture energy: the

✉ Jinhyun Choo
jchoo@hku.hk

[1] Department of Civil Engineering, The University of Hong Kong, Pok Fu Lam, Hong Kong

[2] Earth System Science Programme, The Chinese University of Hong Kong, Sha Tin, Hong Kong

energy released during generation of a unit area of slip surface, which corresponds to the critical energy release rate for mode II fracture. Rice [16] suggested an integration scheme to calculate the shear fracture energy of a material from its post-failure deformation data. Following this suggestion, Wong [17] devised a specific procedure to estimate the shear fracture energy from a triaxial compression test, applying it to data from Westerly granite under different pressures and temperatures. Later, Wong [18] refined the procedure to consider change in the normal stress on the failure plane, studying how the shear fracture energies of rocks depend on the normal stress. The procedure has also been adopted by other researchers to estimate shear fracture energies of hard rocks under various conditions, e.g. [19]. The shear fracture energies of rocks characterized in these studies have been useful for addressing fault rupture problems in seismology, e.g. [20, 21].

Nevertheless, no study seems to have examined shear fracture energies of stiff clays and shales in a similar way, although the theory of Palmer and Rice [6] was originally concerned with overconsolidated clays. So it remains mostly unknown what are the typical values of shear fracture energies of these materials and how much the shear fracture energies would depend on the normal stress on the slip plane.

To fill this knowledge gap, this work characterizes and analyzes shear fracture energies of stiff clays and shales and their related quantities based on triaxial test data from the literature. At the outset, it is noted that here the shear fracture energy is regarded as the surface energy dissipated until the material attains a purely frictional residual strength—being consistent with Palmer and Rice's theory—which can usually be characterized by triaxial/shear-box tests. Some materials, however, manifest "true" residual strength after a very large amount of slip, as a consequence of particle alignment along a localized slip surface [22]. Such residual strength, which is slightly lower than the purely frictional strength, may not be measured by a triaxial/shear-box test but by a ring shear test [23]. Nevertheless, the present work analyzes triaxial test data because drained stress–strain responses under different confining pressures are mostly available from triaxial tests. It would also be debatable whether strength evolution due to particle alignment should be included in fracture energy calculation. A thorough comparison between shear fracture energies of stiff clays and shales characterized by triaxial and ring shear test data is left as a topic of future research.

2 Methodology

2.1 Theory

Consider the softening process during which the shear stress (τ) decreases from the peak strength (τ_p) to the residual strength (τ_r). Palmer and Rice [6] derived that the shear fracture energy ($\mathcal{G}$) is given by

$$\mathcal{G} = \int_0^{\delta_r} [\tau(\delta) - \tau_r]\, \mathrm{d}\delta = (\tau_p - \tau_r)\bar{\delta}. \tag{1}$$

Here, δ is the slip displacement along the shear fracture surface, and δ_r is its value when shear stress reaches the residual shear strength. Also, $\bar{\delta}$ is the characteristic slip displacement, which can be used to analyze the stability and size effect of shear band propagation [6, 8, 11, 13]. For example, the critical length of a shear band (L_{cr}), above which propagation of the shear band can be triggered without a further increase in shear stress, is related to $\bar{\delta}$ as $L_{cr} \propto \sqrt{\bar{\delta}}$ for a shallow-seated slip surface [8, 13] and $L_{cr} \propto \bar{\delta}$ for a deep-seated one [13].

To characterize shear fracture energies from post-peak results of triaxial compression tests, this work adopted the procedure developed by Wong [17, 18]. As shown in Fig. 1, the shear stress and slip displacement can be calculated from triaxial test data as

$$\tau = \frac{\sigma_1' - \sigma_3'}{2}\sin(2\theta), \quad \delta = \frac{\Delta l}{\cos(\theta)}, \tag{2}$$

where σ_1' and σ_3' are the maximum and minimum effective principal stresses, respectively, Δl is the axial displacement of the specimen, and θ is the angle of failure plane from the direction of σ_1.

Equation (1) assumes that shear stress is a function of the slip displacement only, as it was derived from a simple shear problem where the effective normal stress on the slip plane (σ_n') is constant. In a triaxial test where confining pressure is kept constant, however, σ_n' decreases during the softening process. This decrease in $\sigma_{n'}$ makes the amount of stress drop ($\tau_p - \tau_r$) significantly larger than that under a constant normal stress, as illustrated in Fig. 2.

On the basis of an unpublished analysis of Rice, Wong [18] presented a method to consider the effect of evolving σ_n' during triaxial compression. Let us refer to quantities directly obtained from a triaxial test as nominal, denoting them with subscript $(\cdot)_{nom}$. The nominal shear fracture energy is given by

$$\mathcal{G}_{nom} = \int_0^{\delta_r} [\tau(\delta) - \tau_r]_{nom}\, \mathrm{d}\delta = (\tau_p - \tau_r)_{nom} \int_0^{\delta_r} h(\delta)\, \mathrm{d}\delta, \tag{3}$$

where

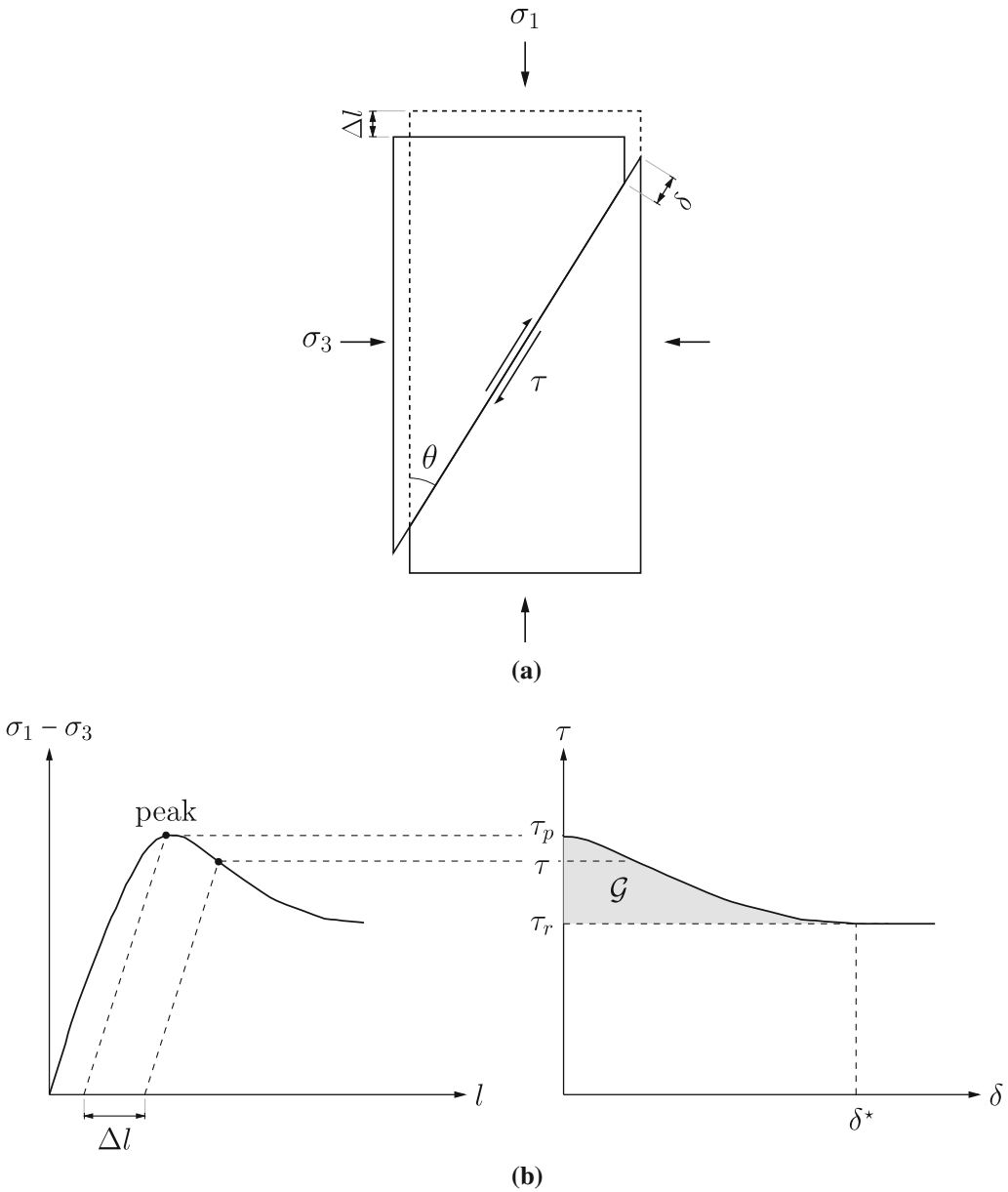

Fig. 1 **a** Configuration of a specimen after formation of a shear band under triaxial compression. **b** Calculation of the shear fracture energy $\mathcal{G}$ from post-failure data in a triaxial compression test. Redrawn from Wong [17]

$$h(\delta) = \frac{[\tau(\delta) - \tau_\mathrm{r}]_\mathrm{nom}}{(\tau_\mathrm{p} - \tau_\mathrm{r})_\mathrm{nom}}. \tag{4}$$

Note that Wong [18] did not distinguish between $(\tau_\mathrm{p} - \tau_\mathrm{r})_\mathrm{nom}$ and $(\tau_\mathrm{p} - \tau_\mathrm{r})$, but later Liu and Rummel [19] did so. To incorporate the dependence of τ_p and τ_r on σ'_n, their relationships are approximated as

$$\tau_\mathrm{p} = A\sigma'_\mathrm{n} + B, \quad \tau_\mathrm{r} = a\sigma'_\mathrm{n} + b, \tag{5}$$

where A, B, a, and b are constants. Then, the shear fracture energy can be calculated as (see Wong [18] for detailed derivation)

$$\mathcal{G} = [(A - a)\sigma'_\mathrm{n} + (B - b)] \int_0^{\delta_\mathrm{r}} f(\delta)h(\delta)\,\mathrm{d}\delta, \tag{6}$$

where

$$f(\delta) = \frac{1 - \beta a}{(1 - \beta A) + \beta(A - a)h(\delta)}, \tag{7}$$

with

$$\beta = \frac{\mathrm{d}\sigma'_\mathrm{n}}{\mathrm{d}\tau} = \tan(\theta) \tag{8}$$

denoting the loading path in a triaxial compression test, as illustrated in Fig. 2.

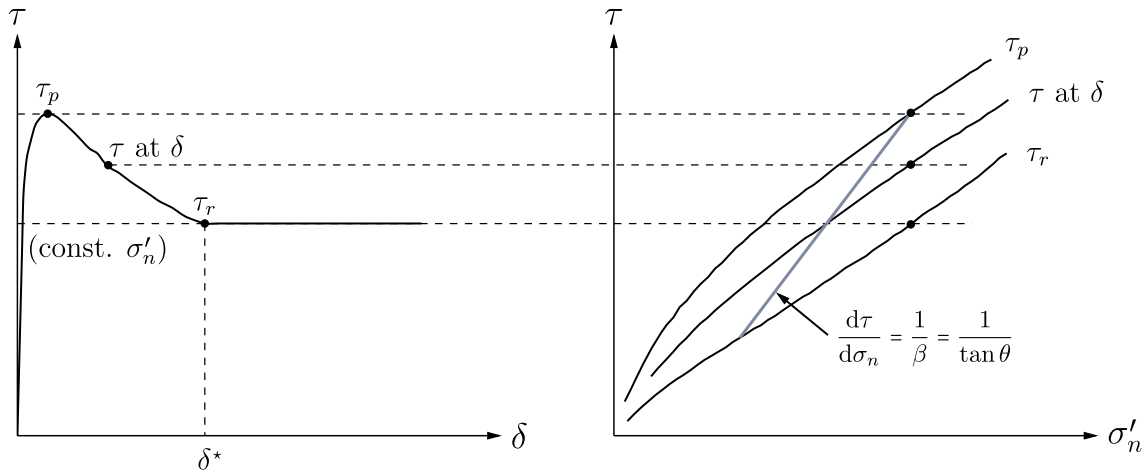

Fig. 2 Comparison of the magnitudes of shear stress drop ($\tau_p - \tau_r$) under constant normal stress (left) and under constant confining pressure in a triaxial compression test (right). The gray line denotes the loading path in a triaxial test. Redrawn from Wong [18]

Importantly, Eq. (6) shows that the dependence of $\mathcal{G}$ on σ'_n is determined by $(A - a)$. This has been experimentally confirmed for rocks (e.g. [18, 19, 24]). Note that the value of $(A - a)$, and so the dependence of $\mathcal{G}$ on σ'_n, can differ significantly by material. Also, because σ'_n in Eq. (6) changes during the softening process, this work will present upper and lower bounds on $\mathcal{G}$, as in Wong [18].

2.2 Data collection and analysis

The foregoing procedure was applied to determine shear fracture energies of various brittle clays and shales from their post-failure deformation data in the literature. To exclude pore pressure effects on the shear fracture energy, this work only considered results from drained triaxial tests. Table 1 summarizes the materials investigated in this work. Most of these materials were compressed only in the direction normal to the bedding plane, while the Opalinus clay [25] and the Tournemire shale [26] samples were loaded in multiple directions. For consistency, this work only used test data from samples loaded in the bedding-plane normal direction. If θ was not provided, it was assumed from Mohr–Coulomb theory. Other details followed the methodology of Wong [18]. To minimize bias, a computer program was developed that automatically calculates shear fracture energies from digitized data. The program was verified by re-calculating the shear fracture energies of different rock specimens in the literature.

3 Results and discussion

3.1 Shear fracture energies

Figure 3 presents the computed values of shear fracture energy with respect to the effective normal stress. It can be

Table 1 Stiff clays and shales investigated in this work

Name	Origin	References
Hambach Clay	Hambach, Germany	[27]
La Biche Shale	Alberta, Canada	[28]
London Clay	London, England	[29]
Nanticoke Clay	Southern Ontario, Canada	[30]
Opalinus Clay	Mont-Terri, Switzerland	[25]
Oxford Clay	South of Bedford, England	[31]
Pietrafitta Stiff Clay	Pietrafitta, Italy	[32, 33]
Roccella Stiff Clay	Calabria, Italy	[34]
Todi Clay	Todi, Italy	[33]
Tournemire Shale	Massif Central, France	[26]
Vallerica Clay	Near River Tiber, North of Rome	[35]

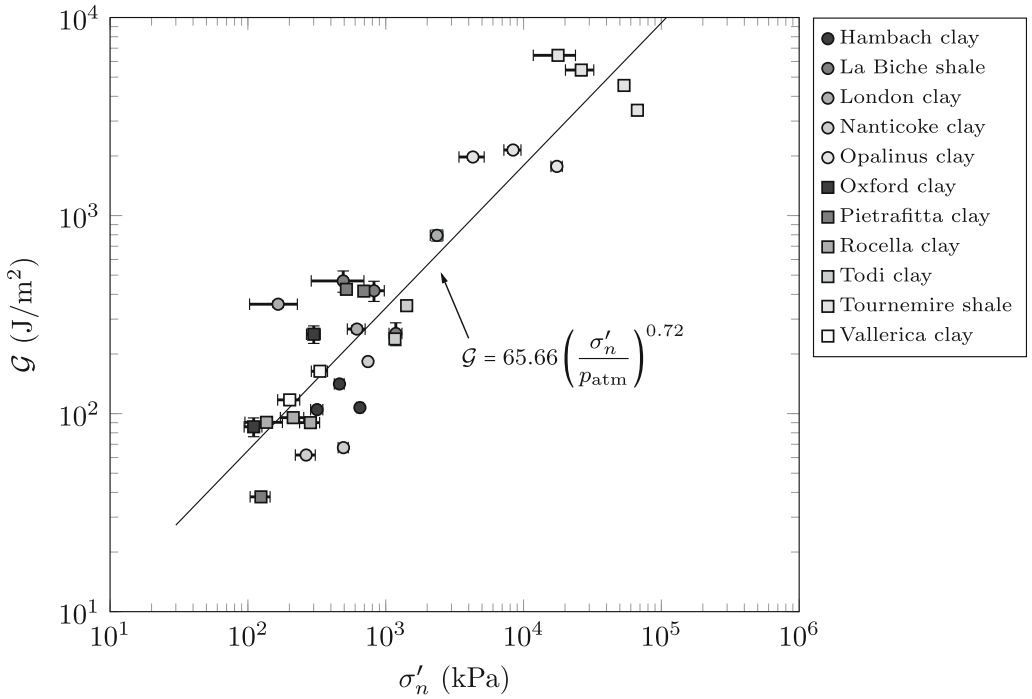

Fig. 3 Shear fracture energies versus effective normal stresses of the stiff clays and shales

seen that the shear fracture energies of these materials vary by orders of magnitude, showing a generally increasing trend with effective normal stresses. Specifically, the shear fracture energies range approximately from 4×10^1 to 7×10^3 J/m^2 when the effective normal stress is varied from 10^2 to 10^5 kPa. Compared with the shear fracture energies of hard rocks such as granite and gabbro [18], those of stiff clays are about two orders of magnitude lower and exhibit a stronger dependence on the effective normal stress. Yet the shear fracture energies of shales are comparable to those of molded gypsum [24].

As shown in Fig. 3, the values of shear fracture energies and normal stresses can be roughly fitted to the following equation

$$\mathcal{G} = 65.66\left(\frac{\sigma'_{\text{n}}}{p_{\text{atm}}}\right)^{0.72} \text{(in J/m}^2\text{)}, \tag{9}$$

where $p_{\text{atm}} = 101.3$ kPa is the atmospheric pressure, which is introduced for dimensional consistency. This equation may provide a first-order estimate of the shear fracture energy of a stiff clay or shale when experimental result is unavailable. Interestingly, Eq. (9) is form-identical to a common empirical relationship between the initial shear stiffness (or shear wave velocity) and the effective normal stress in the loading direction [36, 37]. The value of the exponent, 0.72, is also comparable with the typical values of the shear stiffness/velocity equation for fine-grained soils (e.g. [38, 39]).

Despite the general relationship between the shear fracture energies and effective normal stresses, individual materials exhibit varied degrees of stress dependence. This variance can be attributed to that the value of $(A - a)$ in Eq. (6), which is related to the difference between the peak and residual friction angles, is quite different by materials. Further, because the peak strength envelope of soils and rocks is becoming flatter as the normal stress increases [40, 41], the value of A is small at a relatively high normal stress. This explains why the shear fracture energies of shales at high normal stresses appear nearly stress independent. Therefore, although Eq. (9) may be used for a first-order estimate of the shear fracture energies of stiff clays and shales in general, this equation would not be a proper means for assessing the stress dependence of the shear fracture energy of an individual material. For an individual material, it would be more appropriate to use Eq. (6) or another equation derived in a similar manner.

As an additional note, one should be aware that the shear fracture energy may be scale dependent. For dynamic rupture of rock faults, Abercrombie and Rice [20] and Nielsen et al. [42] have argued that $\mathcal{G} \propto \delta_{\text{tot}}^{1.3}$ and $\mathcal{G} \propto \delta_{\text{tot}}$, respectively, where δ_{tot} is the total slip of a fault. Also, Viesca and Garagash [21] have found $\mathcal{G} \propto \delta_{\text{tot}}^2$ for small earthquake events and $\mathcal{G} \propto \delta_{\text{tot}}^{2/3}$ for large events, elucidating that thermal pressurization is a major mechanism for scaling on fault rupture dynamics. A similar scale-dependence of shear fracture energy may also exist for shear

bands in stiff clays and shales. Probing this hypothesis is believed to be an important future research topic.

3.2 Characteristic slip displacements

Figure 4 shows the characteristic slip displacements of the clay and shale samples with respect to the effective normal stresses. As can be seen, the characteristic slip displacements are smaller than 6 mm, and they appear unrelated to the effective normal stress. This apparent stress-independence suggests that $\bar{\delta}$ can be used for fracture mechanics analysis without consideration of normal stress.

The values of characteristic slip displacements computed herein are close to those calculated from other types of laboratory tests on stiff clays. For example, Palmer and Rice [6] report that the characteristic slip displacements of overconsolidated London clay lie in between 2 and 10 mm, based on the shear test data of Skempton [3] and Skempton and Petley [43]. Also, $\bar{\delta} \approx 3.9$ mm is computed by the authors for the experimental result of Puzrin et al. [9] on an overconsolidated clay in a 2-m-long inclined slope. It is noted that the characteristic slip displacements of clays and shales are greater than those of hard rocks (<1 mm), because they become greater for more ductile materials [12].

It is emphasized again, however, that a scale effect might exist in the characteristic slip displacement. In the context of fault rupture, several studies have suggested $\bar{\delta} \propto \delta_{\text{tot}}$ [44–47]. Because $\bar{\delta} = (\tau_{\text{p}} - \tau_{\text{r}})/\mathcal{G}$, this scale dependence of $\bar{\delta}$ is consistent with $\mathcal{G} \propto \delta_{\text{tot}}^{1.3}$ [20], and exactly the same as $\mathcal{G} \propto \delta_{\text{tot}}$ [42] if τ_{p} and τ_{r} are considered scale independent. Although no investigation has been performed regarding the scale effect of the characteristic slip displacement in shear band propagation in soils and weak rocks, there is limited evidence suggesting a similar scale effect might also exist. For example, from back-analysis of a submarine landslide, Puzrin et al. [10] state that the characteristic slip displacement of the landslide sediment is constrained in between 100 and 160 mm, which is far greater than those estimated from laboratory experiments. If such a scale effect exists, the critical length (L_{cr}) might be underestimated from laboratory tests, leading to an overly conservative stability analysis. This aspect is believed to deserve further investigations.

3.3 True versus nominal values

Figure 5 compares the shear fracture energies and characteristic slip displacements with their nominal values. From Fig. 5a, one can see that the nominal shear fracture energies are consistently greater than the true shear fracture energies, which is a natural consequence of that the nominal stress drop $(\tau_{\text{p}} - \tau_{\text{r}})_{\text{nom}}$ is greater than the true stress drop $(\tau_{\text{p}} - \tau_{\text{r}})$ under a constant normal stress test (cf. Fig. 2).

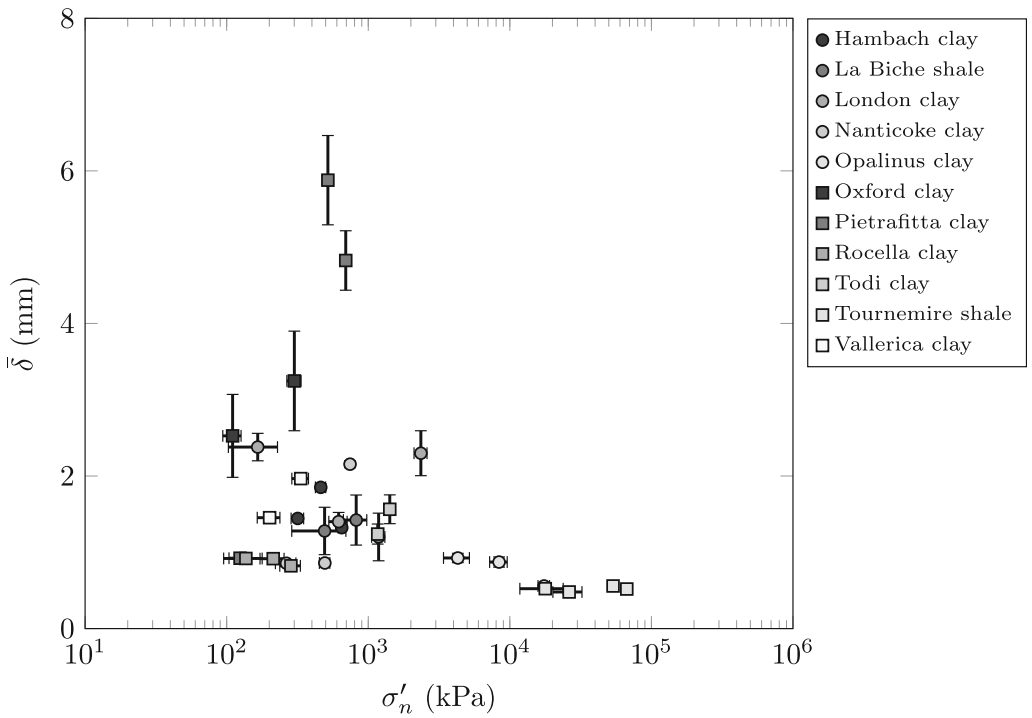

Fig. 4 Characteristic slip displacements versus effective normal stresses of the stiff clays and shales

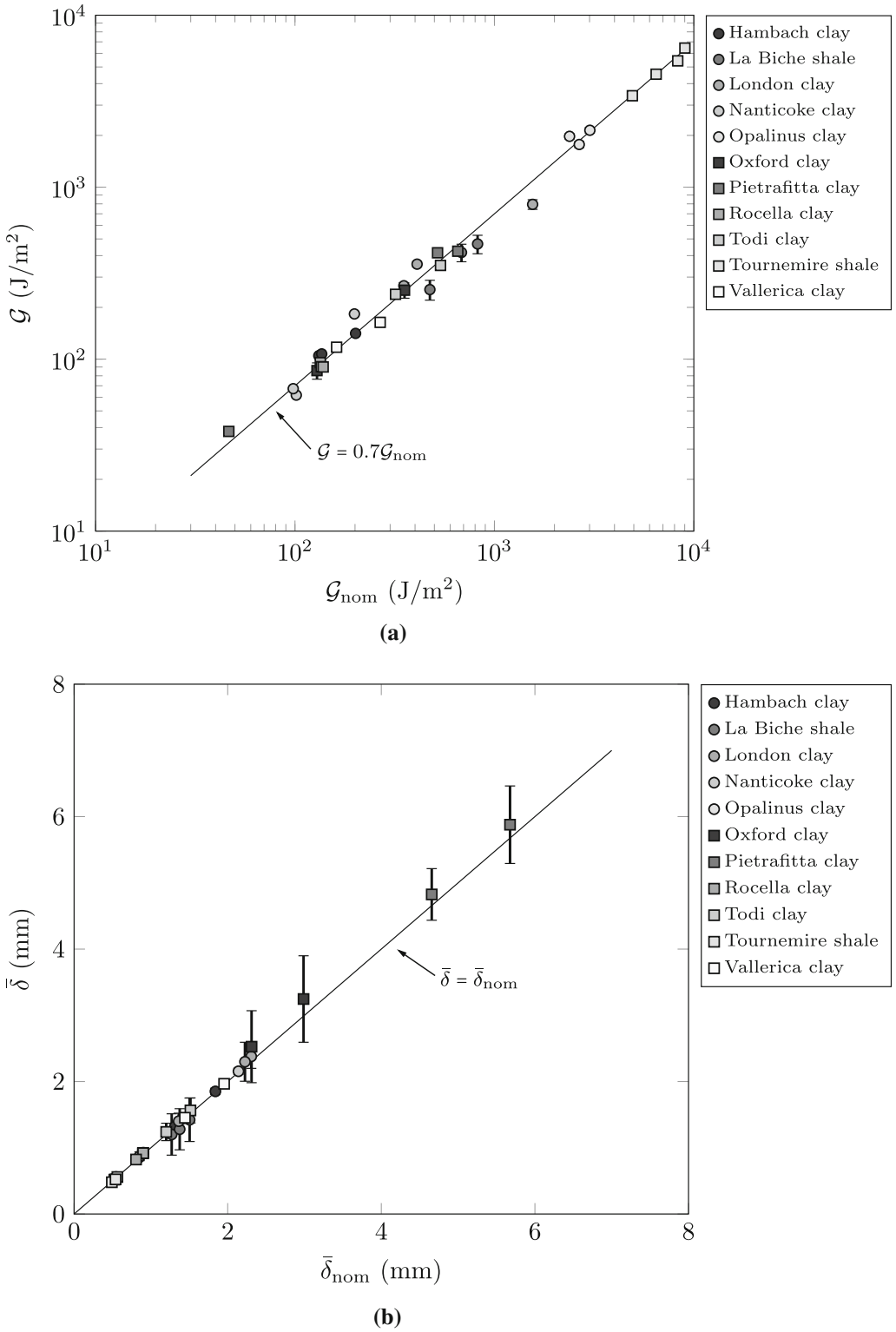

Fig. 5 True versus nominal values: **a** shear fracture energies, and **b** characteristic slip displacements

Remarkably, irrespective of materials and normal stresses, it is found that the shear fracture energies are consistently around 70% of their nominal values. This consistency is interesting because $\mathcal{G}/\mathcal{G}_{\text{nom}}$ of the rocks studied in Wong [18] and Liu and Rummel [19] show non-trivial variances (e.g. $\mathcal{G}/\mathcal{G}_{\text{nom}} \approx 0.35$–$0.5$ for Fichtelbirge granite). By contrast, as shown in Fig. 5b, the characteristic slip displacements are nearly identical to their nominal

values. This similarity, which has also been observed for rocks [19], affirms the stress-independence of the characteristic slip displacements. To summarize,

$$\mathcal{G} \approx 0.7\mathcal{G}_{\text{nom}} \quad \text{and} \quad \bar{\delta} \approx \bar{\delta}_{\text{nom}}. \tag{10}$$

These approximations may be useful because it is much easier to calculate nominal values than true values.

4 Conclusion

Based on the results above, the following conclusions can be drawn regarding the shear fracture energies and characteristic slip displacements of stiff clays and shales estimated from triaxial tests:

1. The shear fracture energies generally increase with the effective normal stress on the slip plane, varying by orders of magnitude—approximately from 4×10^1 to 7×10^3 J/m^2—in the range of effective normal stresses from 10^2 to 10^5 kPa.
2. An empirical Eq. (9) may provide a first-order estimate of the shear fracture energy under a given effective normal stress.
3. The characteristic slip displacements are smaller than 6 mm, and they appear independent of the effective normal stress.
4. Compared with their nominal values calculated without considering the change of normal stress in triaxial tests, the shear fracture energies are approximately 70% of the nominal values, whereas the characteristic slip displacements are nearly identical to the nominal ones.

These findings can be useful for fracture mechanics analysis of shear band propagation in stiff clays and shales. Special care should be exercised, however, when the material of interest would attain its residual strength after a very large slip displacement that cannot be imposed in triaxial tests. It is also emphasized that future work is necessary to elucidate scale effects on the shear fracture energies and characteristic slip displacements of these materials.

Acknowledgements The authors wish to thank the two anonymous reviewers for their insightful and constructive comments. Financial support for this work was provided by the Research Grants Council of Hong Kong through the Early Career Scheme (27205918), General Research Fund (17201419), and the NSFC/RGC Joint Research Scheme (N_CUHK430/16).

References

1. Rudnicki JW, Rice JR (1975) Conditions for the localization of deformation in pressure-sensitive dilatant materials. J Mech Phys Solids 23(6):371–394
2. Vardoulakis I, Goldscheider M, Gudehus G (1978) Formation of shear bands in sand bodies as a bifurcation problem. Int J Numer Anal Methods Geomech 2(2):99–128
3. Skempton AW (1964) Long-term stability of clay slopes. Géotechnique 14(2):77–102
4. Bjerrum L (1967) Progressive failure in slopes of overconsolidated plastic clay and clay shales. J Soil Mech Found Div 93:1–49
5. Bishop AW (1968). Progressive failure—with special reference to the mechanism causing it. In: Proceedings of the geotechnical conference, Vol. 2. Norwegian Geotechnical Institute, pp. 142–150
6. Palmer AC, Rice JR (1973) The growth of slip surfaces in the progressive failure of over-consolidated clay. Proc R Soc Lond A Math Phys Sci 332(1591):527–548
7. Puzrin AM, Germanovich LN, Kim S (2004) Catastrophic failure of submerged slopes in normally consolidated sediments. Géotechnique 54(10):631–643
8. Puzrin AM, Germanovich LN (2005) The growth of shear bands in the catastrophic failure of soils. Proc R Soc A Math Phys Eng Sci 461(2056):1199–1228
9. Puzrin AM, Germanovich LN, Friedli B (2016) Shear band propagation analysis of submarine slope stability. Géotechnique 66(3):188–201
10. Puzrin AM (2016) Simple criteria for ploughing and runout in post-failure evolution of submarine landslides. Can Geotech J 53(8):1305–1314
11. Quinn P, Diederichs M, Rowe R, Hutchinson D (2011) A new model for large landslides in sensitive clay using a fracture mechanics approach. Can Geotech J 48(8):1151–1162
12. Quinn P, Diederichs M, Rowe R, Hutchinson D (2012) Development of progressive failure in sensitive clay slopes. Can Geotech J 49(7):782–795
13. Viesca RC, Rice JR (2012) Nucleation of slip-weakening rupture instability in landslides by localized increase of pore pressure. J Geophys Res Solid Earth 117(B3):1–21
14. Fei F, Choo J (2020) A phase-field model of frictional shear fracture in geologic materials. Comput Methods Appl Mech Eng 369:113265
15. Fei F, Choo J (2021) Double-phase-field formulation for mixed-mode fracture in rocks. Comput Methods Appl Mech Eng 376:113655
16. Rice JR (1980) The mechanics of earthquake rupture. In: Physics of the earth's interior. Italian Physical Society, pp 555–649
17. Wong T-F (1982) Shear fracture energy of Westerly granite from post-failure behavior. J Geophys Res Solid Earth 87(B2):990–1000
18. Wong T (1986) On the normal stress dependence of the shear fracture energy. In: Earthquake source mechanics, vol 37. American Geophysical Union, pp 1–11
19. Liu Z, Rummel F (1990) Shear fracture energy of rock at high pressure and high temperature. Phys Chem Earth 17:99–109
20. Abercrombie RE, Rice JR (2005) Can observations of earthquake scaling constrain slip weakening? Geophys J Int 162(2):406–424
21. Viesca RC, Garagash DI (2015) Ubiquitous weakening of faults due to thermal pressurization. Nat Geosci 8(11):875–879
22. Mitchell JK, Soga K (2005) Fundamentals of soil behavior. Wiley, Hoboken
23. Bishop AW, Green GE, Garga VK, Andresen A, Brown JD (1971) A new ring shear apparatus and its application to the measurement of residual strength. Géotechnique 21(4):273–328
24. Mutlu O, Bobet A (2006) Slip propagation along frictional discontinuities. Int J Rock Mech Min Sci 43(6):860–876
25. Favero V, Ferrari A, Laloui L (2018) Anisotropic behaviour of Opalinus Clay through consolidated and drained triaxial testing in saturated conditions. Rock Mech ICS Rock Eng 51(5):1305–1319

26. Niandou H, Shao J, Henry J, Fourmaintraux D (1997) Laboratory investigation of the mechanical behaviour of Tournemire shale. Int J Rock Mech Min Sci 34(1):3–16
27. Shi X, Herle I, Yin J (2018) Laboratory study of the shear strength and state boundary surface of a natural lumpy soil. J Geotech Geoenviron Eng 144(12):04018093
28. Wong RCK (1998) Swelling and softening behaviour of La Biche shale. Can Geotech J 32(2):206–221
29. Bishop AW, Webb DL, Lewin PI (1965) Undisturbed samples of London Clay from the Ashford Common shaft: strength-effective stress relationships. Géotechnique 15(1):1–31
30. Lo K (1972) An approach to the problem of progressive failure. Can Geotech J 9(4):407–429
31. Parry RHG (1972) Some properties of heavily overconsolidated Oxford Clay at a site near Bedford. Geotechnique 22(3):485–507
32. Callisto L, Rampello S (2002) Shear strength and small-strain stiffness of a natural clay under general stress conditions. Géotechnique 52(8):547–560
33. Burland J, Rampello S, Georgiannou V, Calabresi G (1996) A laboratory study of the strength of four stiff clays. Géotechnique 46(3):491–514
34. Mandaglio M, Moraci N, Rosone M, Farulla CA (2016) Experimental study of a naturally weathered stiff clay. Can Geotech J 53(12):2047–2057
35. Callisto L, Rampello S (2004) An interpretation of structural degradation for three natural clays. Can Geotech J 41(3):392–407
36. Hardin BO, Richart FE Jr (1963) Elastic wave velocities in granular soils. J Soil Mech Found Eng 89:33–65
37. Santamarina JC, Klein KA, Fam MA (2001) Soils and waves. Wiley, New York
38. Rampello S, Viggiani G, Amorosi A (1997) Small-strain stiffness of reconstituted clay compressed along constant triaxial effective stress ratio paths. Géotechnique 47(3):475–489
39. Choo J, Jung Y-H, Chung C-K (2011) Effect of directional stress history on anisotropy of initial stiffness of cohesive soils measured by bender element tests. Soils Found 51(4):737–747
40. Atkinson J (2007) Peak strength of overconsolidated clays. Géotechnique 57(2):127–135
41. Barton N (1976) The shear strength of rock and rock joints. Int J Rock Mech Min Sci Geomech Abst 13(9):255–279
42. Nielsen S, Spagnuolo E, Violay M, Smith S, Di Toro G, Bistacchi A (2016) G: Fracture energy, friction and dissipation in earthquakes. J Seismol 20(4):1187–1205
43. A. W. Skempton and D. J. Petley (1968). The strength along structural discontinuities in stiff clays. In: Proceedings of the geotechnical conference Oslo, 1967, vol 2. Norwegian Geotechnical Institute, pp 29–46
44. Dalguer L, Irikura K, Riera J (2003) Generation of new cracks accompanied by the dynamic shear rupture propagation of the 2000 Tottori (Japan) earthquake. Bull Seismol Soc Am 93(5):2236–2252
45. Pulido N, Kubo T (2004) Near-fault strong motion complexity of the 2000 Tottori earthquake (Japan) from a broadband source asperity model. Tectonophysics 390(1–4):177–192
46. Tinti E, Spudich P, Cocco M (2005) Earthquake fracture energy inferred from kinematic rupture models on extended faults. J Geophys Res Solid Earth 110(B12):1–25
47. Burjánek J, Zahradník J (2007) Dynamic stress field of a kinematic earthquake source model with k-squared slip distribution. Geophys J Int 171(3):1082–1097